Molecular Systems Biology 5; Article number 250; doi:10.1038/msb.2009.5
Citation: ***Molecular Systems Biology*** **5:250**

www.molecularsystemsbiology.com

molecular systems biology

Force- and kinesin-8-dependent effects in the spatial regulation of fission yeast microtubule dynamics

Christian Tischer[1,*], Damian Brunner[2] and Marileen Dogterom[1]

[1] Bio-assembly and Organization, FOM Institute for Atomic and Molecular Physics (AMOLF), Amsterdam, The Netherlands and [2] European Molecular Biology Laboratory, Heidelberg, Germany
* Corresponding author. European Molecular Biology Laboratory, Heidelberg, Germany. Tel.: +49 6221 387 8638; Fax: +49 6221 387 8306;
E-mail: Christian.Tischer@EMBL.DE

Received 22.8.08; accepted 23.12.08

Microtubules (MTs) are central to the organisation of the eukaryotic intracellular space and are involved in the control of cell morphology. For these purposes, MT polymerisation dynamics are tightly regulated. Using automated image analysis software, we investigate the spatial dependence of MT dynamics in interphase fission yeast cells with unprecedented statistical accuracy. We find that MT catastrophe frequencies (switches from polymerisation to depolymerisation) strongly depend on intracellular position. We provide evidence that compressive forces generated by MTs growing against the cell pole locally reduce MT growth velocities and enhance catastrophe frequencies. Furthermore, we find evidence for an MT length-dependent increase in the catastrophe frequency that is mediated by kinesin-8 proteins (Klp5/6). Given the intrinsic susceptibility of MT dynamics to compressive forces and the widespread importance of kinesin-8 proteins, we propose that similar spatial regulation of MT dynamics plays a role in other cell types as well. In addition, our systematic and quantitative data should provide valuable input for (mathematical) models of MT organisation in living cells.
Molecular Systems Biology 17 March 2009; doi:10.1038/msb.2009.5
Subject Categories: simulation and data analysis; cell and tissue architecture
Keywords: catastrophes; fission yeast; forces; kinesin-8; microtubules

Introduction

Microtubules (MTs) are dynamic protein polymers that change their length by switching between growing and shrinking states in a process termed 'dynamic instability' (Mitchison and Kirschner, 1984; Desai and Mitchison, 1997). It is important to understand how dynamic instability is regulated, because this affects MT length (Verde *et al*, 1992; Dogterom and Leibler, 1993) and intracellular organisation (Kirschner and Mitchison, 1986; Hayles and Nurse, 2001), as well as the ability of MTs to exert pushing and pulling forces (Inoue and Salmon, 1995; Dogterom *et al*, 2005). Several proteins have been characterised that globally affect MT dynamics and catastrophe rates (Howard and Hyman, 2007), but it is a largely open question how such regulation is achieved locally, in response to spatially varying biochemical cues and/or mechanical effects induced by the shape and size of cells. In fact, in addition to global regulation, it has been reported that catastrophe frequencies can be locally enhanced, for example close to the periphery of animal cells (Komarova *et al*, 2002; Mimori-Kiyosue *et al*, 2005). There are several ways by which such a local catastrophe enhancement could be accomplished: (activity) gradients of destabilising MT-associated proteins (Niethammer *et al*, 2004) and/or MT length-dependent mechanisms (Dogterom *et al*, 1996) would lead to a gradual catastrophe enhancement when approaching the cell boundary. On the other hand, force-induced effects that may result from growing MTs pushing against the cell boundary (Dogterom and Yurke, 1997; Janson *et al*, 2003; Janson and Dogterom, 2004) would lead to an abrupt catastrophe enhancement once contact with the cell boundary has been made. A similar abrupt change would be expected in case there is an MT-destabilising factor associated locally with the membrane (Mimori-Kiyosue *et al*, 2005). To distinguish between long- and short-range mechanisms requires quantitative and spatially resolved measurements of the catastrophe frequency inside living cells. In mammalian cells, this is often a challenging task because MT networks are quite dense and reference points such as the cell boundary in interphase or chromosomes in mitosis are dynamic structures themselves.

Another challenge is that catastrophes appear to be stochastic events that are governed by an average rate (Odde, 1995; Howell *et al*, 1997). This has two consequences: statistical accuracy is a serious issue when investigating catastrophe frequencies, and, the stochastic nature of the process makes it very difficult to avoid picking a subset of events when examining data by visual inspection.

In this paper, we present quantitative investigations of spatial MT catastrophe regulation in interphase fission yeast (*Schizosaccharomyces pombe*) cells with high statistical accuracy (Hayles and Nurse, 2001). Fission yeast is an excellent model system, because MTs are well organised and the rigid cylindrical cell wall makes it possible to accurately assign catastrophes to specific locations within the cell (Figure 1A and B). In interphase cells, MTs are organised into 3–6 bundles, consisting of 2–6 antiparallel MTs per bundle (Hoog *et al*, 2007; Hagan, 1998), which are usually (but not always) connected to the nucleus (Carazo-Salas and Nurse, 2006; Zheng *et al*, 2006; Daga *et al*, 2006a). MT minus ends are generally found close to the nucleus within the central overlap zone of the MTs, whereas dynamic plus tips grow and shrink between the nucleus and the cell poles (Drummond and Cross, 2000; Tran *et al*, 2001). Catastrophe events are mainly restricted to the regions of the two cell poles by an unknown mechanism. This local regulation of MT catastrophes is, however, crucial for the maintenance of correct fission yeast morphology and intracellular organisation (Beinhauer *et al*, 1997; Mata and Nurse, 1997; Browning *et al*, 2000; Brunner and Nurse, 2000; Hayles and Nurse, 2001; Tran *et al*, 2001; Sawin and Snaith, 2004; Tolic-Norrelykke *et al*, 2005; Daga *et al*, 2006b). To obtain good statistics and to ensure unbiased observations, we developed fully automated image analysis software that generates spatially resolved maps of MT dynamics from movies of GFP-labelled MTs in fission yeast (see Supplementary information). Our spatially resolved measurements show that there is both local enhancement of the catastrophe frequency specifically at cell poles as well as long-range modulation before the cell pole is reached. We find several indications that the local regulation at the cell pole is (at least in part) due to compressive forces that build up when bundle tips hit the cell pole. In addition, we find evidence that the long-range catastrophe regulation is a MT length-dependent effect mediated by the kinesin-8 proteins Klp5/6. Since physical boundaries as well as kinesin-8 proteins are also present in other eukaryotic systems, we think that the relevance of our findings reaches beyond the fission yeast model system.

Results

Spatial dependence of MT dynamics

We started by monitoring MT dynamics only in cells of similar size (with a half length of $5 \pm 0.5\,\mu m$). Our software was designed to specifically monitor catastrophes of the longest MTs in each bundle (the 'bundle tips'; see Figure 1B), which we called 'bundle tip catastrophes'. The dynamics of the longest MTs in a bundle are particularly relevant as they are the ones that make contact with the cell walls, where they can deliver proteins (Mata and Nurse, 1997; Feierbach *et al*, 2004) and generate pushing forces that mediate nuclear centring (Tran *et al*, 2001; Tolic-Norrelykke *et al*, 2005; Daga *et al*, 2006b).

In agreement with earlier results obtained by visual inspection (Brunner and Nurse, 2000), the software reported that the great majority of bundle tip catastrophes (N_{cat}) occur

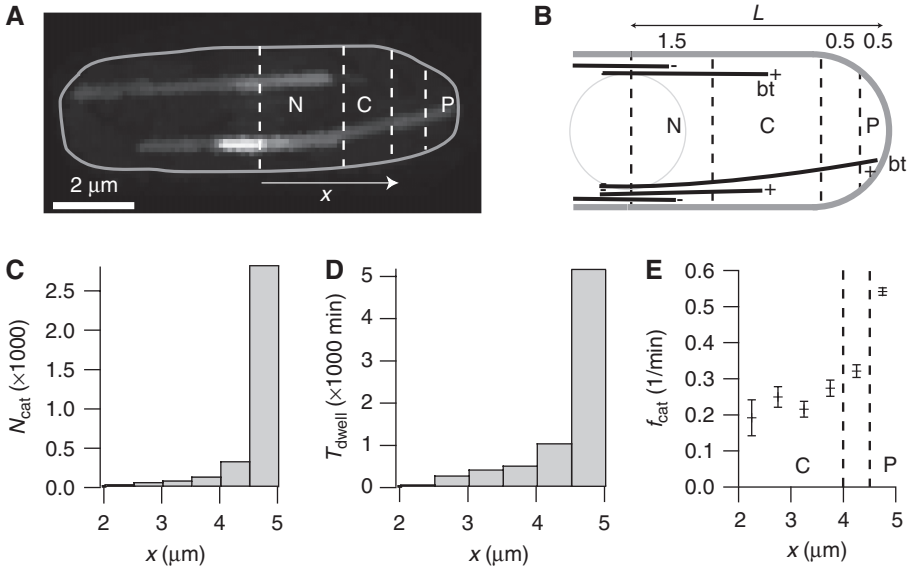

Figure 1 Spatially resolved catastrophe frequency measurements in fission yeast. (**A**) *z*-maximum projection of a confocal stack of images of an interphase fission yeast cell expressing GFP-tubulin (N=nuclear region; C=cytoplasmic region; P=cell pole region; *x*=distance from cell centre). (**B**) Scheme of MT organisation, including definitions of parameters and intracellular regions. Numbers are lengths in micrometres (bt=MT bundle tip; *L*=cell half length). (**C**) Number of catastrophes $N_{cat}(x)$ and (**D**) bundle-tip dwell times $T_{dwell}(x)$ as observed in 160 cells with $L \pm \Delta L = 5 \pm 0.5\,\mu m$. (**E**) Local catastrophe frequency $f_{cat}(x) = N_{cat}(x)/T_{dwell}(x)$. Here and in other figures, due to the averaging over a certain cell size range, the *x* coordinate comprises values within the interval $[x - \Delta L, x + \Delta L]$; errors for f_{cat} are computed as $\sqrt{N_{cat}}/T_{dwell}$ assuming a Poisson process.

at the cell poles (Figure 1C). This is sometimes interpreted as an indicator of spatial catastrophe regulation. However, observing a large number of catastrophes could simply be the consequence of the fact that the majority of bundle tips is found at the cell poles. To distinguish between these possibilities, our software also performed spatially resolved measurements of the time bundle tips were observed growing in a certain region, which we termed the dwell time T_{dwell} (Figure 1D; Supplementary Figure S1). This allowed us to compute a spatially resolved *catastrophe frequency* $f_{cat}(x)=N_{cat}(x)/T_{dwell}(x)$, where x is the distance from the cell centre. $f_{cat}(x)$ is the probability per unit time that individual MTs switch from a growing to a shrinking state at position x (Walker *et al*, 1988). Note that global (spatially averaged) values of f_{cat} have been measured in fission yeast before (Tran *et al*, 2001; Busch and Brunner, 2004). Using this methodology, we found a strong enhancement of not only the number of catastrophes but also f_{cat} itself at the cell pole (Figure 1E). To investigate whether this effect really depended on cell pole proximity rather than on the distance to the cell centre, we measured f_{cat} in cells of different lengths. The half length (L) of fission yeast under laboratory conditions ranges from about 3 to 7 μm (Sveiczer *et al*, 1996), where the longer length regime is difficult to study, because cells are entering mitosis. To facilitate the investigation of a possible long-range regulation of MT dynamics, we administered low doses of the drug hydroxyurea (HU), which significantly increased cell length without altering MT catastrophe, growth or shrinkage dynamics (see Supplementary information). In Figure 2A, we show the results for f_{cat} as a function of cell half length L and distance from the cell centre x (we obtained similar results with cells that were elongated using mutations in cell cycle regulatory genes instead of HU treatment, see Supplementary Figure S8). If we focus on a given distance from the cell centre, we find that f_{cat} at the poles is generally larger than the f_{cat} of MTs that roughly have the same length but that are not yet at the cell pole (Figure 2B). This indicates that there indeed exists a cell pole-specific f_{cat} enhancement. Note however that the abrupt increase of f_{cat} at the poles that is observed in short cells (Figure 1E) is less obvious in longer cells (Figure 2B and C). Interestingly, the data also show a gradual increase of f_{cat} for MTs still growing in the cytoplasmic region (Figure 2A–C) (note: we use the terminology 'cytoplasmic region' to classify MTs that are more than 1 μm away from the cell poles; we do not distinguish whether these MTs are in contact with cell walls or not). To further establish this spatial dependence of f_{cat} in the cytoplasmic region (and exclude that this is a unique feature of overly long cells), we defined a proximal and distal cellular region, where the distal region is excluding the last 2 μm towards the cell pole (Figure 2D). For both cells of normal sizes ($L<7$ μm) and for elongated cells ($L>7$ μm), we find that f_{cat} is significantly higher in the distal region. We in addition devised software to automatically measure the velocity at which the tips of bundles moved through the cytoplasmic region (see Supplementary Figure S4B). In contrast to the f_{cat} measurements, we found no evidence for a strong spatial variation of cytoplasmic growth and shrinkage velocities (Figure 3A–C).

Detailed analysis of MT dynamics at cell poles

In search for a mechanistic explanation for the cell pole specific f_{cat} enhancement, visual inspection of movies suggested to us that the probability for catastrophes was higher when both tips of a bundle were simultaneously in contact with both cell poles. Figure 4A shows an example where the arrival of the opposite bundle tip at the opposite cell pole seemed to trigger catastrophes of both bundle tips. Given the stochastic nature of MT catastrophes, this sequence of events could be coincidental. To rigorously test whether there was an effect, we measured f_{cat} in the cell pole region while keeping automatically track of whether the other bundle tip was close to the opposite cell pole or not (P_P versus P_C, Figure 4B; Supplementary Figure S4A). The quantification revealed that f_{cat} was indeed significantly enhanced in the P_P as compared with the P_C situation (Figure 4C; Supplementary Figure S7B). In contrast, the f_{cat} of MTs growing through the cytoplasmic region was similar no matter whether the other

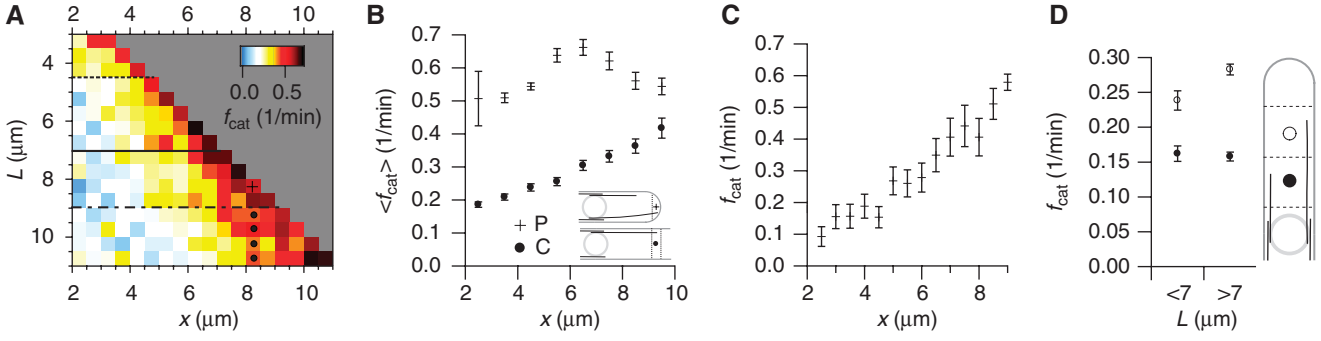

Figure 2 Spatially resolved f_{cat} measurements in wild-type cells as a function of distance to the cell centre (x) in cells with different half lengths L. (**A**) $f_{cat}(x,L)$. The solid horizontal line indicates the L at which cells normally undergo mitosis under laboratory conditions. Longer cells were obtained by delaying mitosis through hydroxyurea treatment. The cross and circles refer for one specific x to the presentation of the data in (B). Dash and dash-dot horizontal lines indicate data shown in Figures 1E and 2C, respectively. Statistics: $N_{cat}=10878$; $N_{cells}=533$; here and in other figures, data for large L are more noisy because of less statistics; see also Supplementary Figure S2. (**B**) Comparison of f_{cat} at the pole (crosses) in cells of different lengths ($L=x$) to f_{cat} in the cytoplasmic region at same position x in longer cells (circles; averaged over all cells with $L>x+1$ μm). (**C**) $f_{cat}(x)$ for cells with $L=9\pm0.5$ μm. (**D**) Average f_{cat} in cytoplasmic regions proximal ($x_1<x<x_2$) and distal ($x_2<x<x_3$) to the cell centre, for cells with normal ($L<7$ μm) and elongated ($L>7$ μm) sizes. $x_1=1.5$ μm; $x_3=L-2$ μm; $x_2=(x_1+x_3)/2$. Statistics: $L<7$ μm: $N_{cat}=492$; $N_{cells}=339$; $L>7$ μm; $N_{cat}=1826$; $N_{cells}=286$.

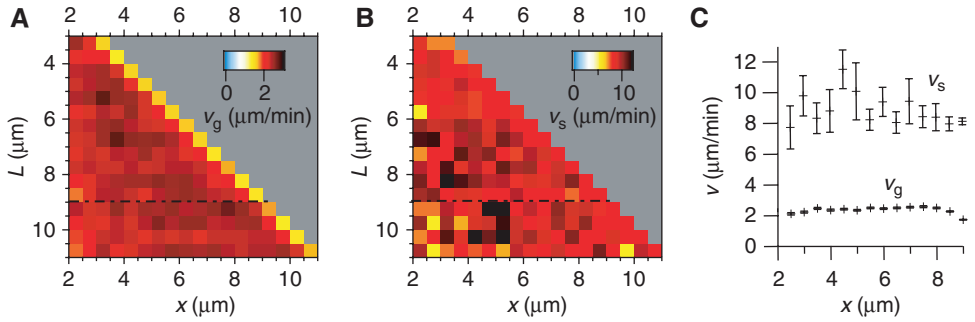

Figure 3 Spatially resolved bundle tip velocity measurements in wild-type cells. (**A**, **B**) Bundle tip velocities for growing (v_g) and shrinking (v_s) microtubules. (**C**) Growth and shrinkage velocities for cells with $L=9\pm0.5$ μm, corresponding to dash-dot horizontal lines in (A, B).

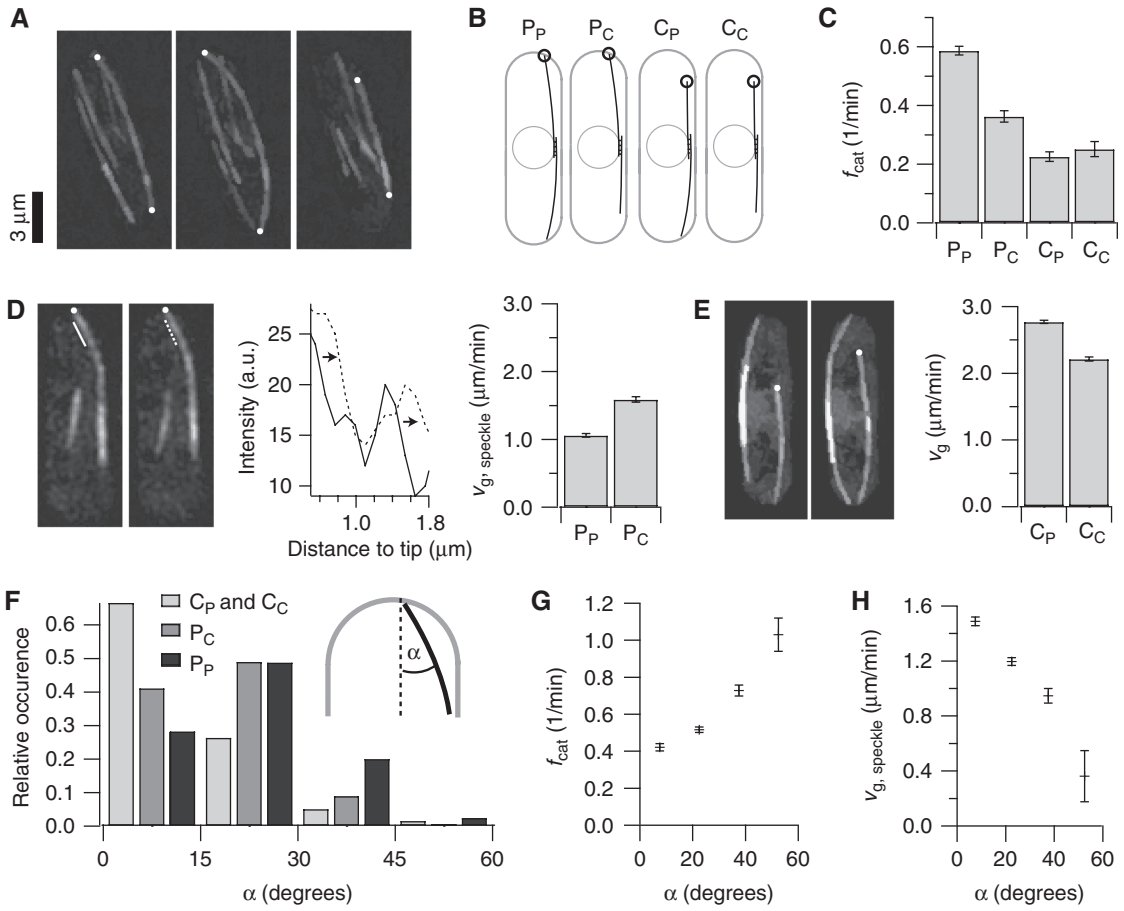

Figure 4 Microtubule dynamics at the poles of untreated cells with $3\,\mu m\leqslant L\leqslant 7\,\mu m$. (**A**) Sequence of GFP-tubulin *z*-maximum projections (Δt=32 s); white dots indicate the MT bundle tips referred to in the text. (**B**, **C**) Catastrophe frequency depending on bundle tip position (P=pole, C=cytoplasm) and depending on position of the opposite bundle tip (subscript P or C). Statistics: N_{cat}: P_P 1566; P_C 346; C_P 192; C_C 97. (**D**) Left panel: sequence of GFP-tubulin *z*-maximum projections (Δt=8 s). Middle panel: intensity profiles following the bundle axis in 3D (see Supplementary information). Solid and dashed lines correspond to images in (D). Right panel: growth velocity of bundle tips at cell poles as measured by 3D GFP-tubulin speckle motion, depending on opposite bundle tip position (mean ± s.e.m. from 6455 P_P and 3234 P_C events in 272 cells). (**E**) Left panel: sequence of GFP-tubulin *z*-maximum projections (Δt=24 s); white dots mark a growing bundle tip. Right panel: velocities at which growing bundle tips move through the cytoplasmic region, depending on the position of the opposite bundle tip (mean ± s.e.m. from 4089 C_P and 1763 C_C events in 272 cells). (**F**) Histogram of angles between bundle tips and the long axis of the cell (statistics: C_P and C_C 6410 events; P_C 7532 events; P_P 18485 events). 3D angles were computed using the (*x*,*y*,*z*) positions of the bundle tip and of a point about 0.8 μm behind the bundle tip (see inset and Supplementary information). (**G**, **H**) f_{cat} and bundle tip growth velocity as a function of angle.

bundle tip was at the cell pole or not (C_P versus C_C). Note that in a recent study a higher f_{cat} was found in the C_P (compared to C_C) situation in cells where the nucleus was displaced to one side of the cell by centrifugation (Daga *et al*, 2006b). We do not find such an effect in our cells. The difference could, however, simply be a statistical issue as the total observation time of

cytoplasmic MTs in the study by Daga *et al* was rather short (33 min versus 1204 min in this study). To further investigate the difference between the P_P and P_C situation, we monitored MT growth velocities in both cases. This poses some technical difficulty because MT growth against the cell wall does not necessarily result in MT tip displacement (Drummond and Cross, 2000; Tran *et al*, 2001; Grallert *et al*, 2006). However, quantification of GFP-tubulin speckle translocation (Tran *et al*, 2001) revealed that the MT growth velocity at the pole was significantly reduced in the P_P as compared with the P_C situation (Figure 4D; Supplementary Figure S3C). When we monitored the velocity at which bundle tips moved through the cytoplasmic region we found the opposite effect: tip movement through the cytoplasmic region was faster in the presence of opposite pole contact (Figure 4E). We in addition found that the angles at which the bundle tips at the cell poles were growing with respect to the long axis of the cell were larger in the P_P than in the P_C case (and lowest for MTs that were growing in the cytoplasmic region) (Figure 4F). These large angles correlated with both a strong enhancement of f_{cat} and a strong reduction of MT growth velocity (Figure 4G and H; see also Supplementary Figure S7C). We interpret the reduction in velocity at the cell poles as the result of force-induced effects (see Discussion below). However, an alternative explanation for the reduced velocity in the P_P case may be that the overall polymer mass in the cell is higher, leading to a lower tubulin concentration and a global reduction in the growth velocity. When we measured the growth velocities of cytoplasmic bundle tips in the C_C situation, depending on whether there was a neighbouring P_P or P_C bundle, we found however no significant difference (P_P: v_g=2.28 ± 0.05 μm/min, N=469; P_C: v_g=2.29 ± 0.06 μm/min, N=449).

Spatial dependence of MT dynamics in Klp5/6 deletion strains

Next, we investigated whether the observed long-range increase of f_{cat} depended on the presence of the fission yeast kinesin-8 proteins Klp5 and Klp6. This was motivated by recent *in vitro* experiments on the depolymerisation activity of the budding yeast kinesin-8 protein Kip3 (Varga *et al*, 2006) on GMPCPP-stabilised MTs. These experiments led to speculations that kinesin-8 proteins could have the capability to increase f_{cat} of non-stabilised MTs in an MT length-dependent manner (Gardner *et al*, 2008; Stumpff *et al*, 2008). Corroborating observations by West *et al* (2001), bundles in *klp5Δklp6Δ* cells seemed on average longer than in wild-type cells (Supplementary Figure S2A and D). Quantification of bundle tip dynamics in *klp5Δklp6Δ* cells showed that f_{cat} was overall about 40% reduced as compared with wild-type cells (Figure 5A). More interestingly, we found that the long-range f_{cat} increase in the cytoplasmic region was strongly reduced in *klp5Δklp6Δ* cells (Figure 5A–D). Also the cell length dependence of f_{cat} at cell poles was strongly reduced as compared with wild-type cells (Figure 5B). There was however still a clear difference in f_{cat} for MTs at the pole and MTs not yet at the pole for a given value of x (Figure 5B). We also measured the spatial dependence of the growth and shrinkage velocities in these cells (Supplementary Figure S3). We found that the average cytoplasmic growth velocities of growing bundle tips were overall about 15% reduced in *klp5Δklp6Δ* cells (v_g^{wt}=2.42 ± 0.01 μm/min (N=11578); $v_g^{Klp5/6\Delta}$=2.05 ± 0.02 μm/min (N=3677)), whereas shrinkage velocities were not significantly different (v_s^{wt}=8.7 ± 0.2 μm/min (N=613); $v_s^{Klp5/6\Delta}$=8.7 ± 0.3 μm/min (N=173)).

Analysis of Klp5/6 distribution along MTs

The data presented above indicate that Klp5/Klp6 proteins preferentially promote catastrophes at positions far from the cell centre, consistent with the idea that these proteins induce an MT length-dependent effect. To gain more insight into the mechanism, we investigated the localisation of Klp5/Klp6 along MTs. Although it has been shown that Klp5 and Klp6 colocalise on interphase MTs (West *et al*, 2001; Garcia *et al*, 2002), presumably due to heterodimerisation (Garcia *et al*, 2002), a detailed analysis of their spatial distribution is missing. We revisited Klp5/Klp6 localisation by monitoring Klp5-GFP and Klp6-GFP expressed under control of the respective endogenous promoter (West *et al*, 2001). Visual inspection of *z*-maximum projections of Klp5/6-GFP indicated that the intensity of Klp5/6-GFP was higher on the tips of MTs

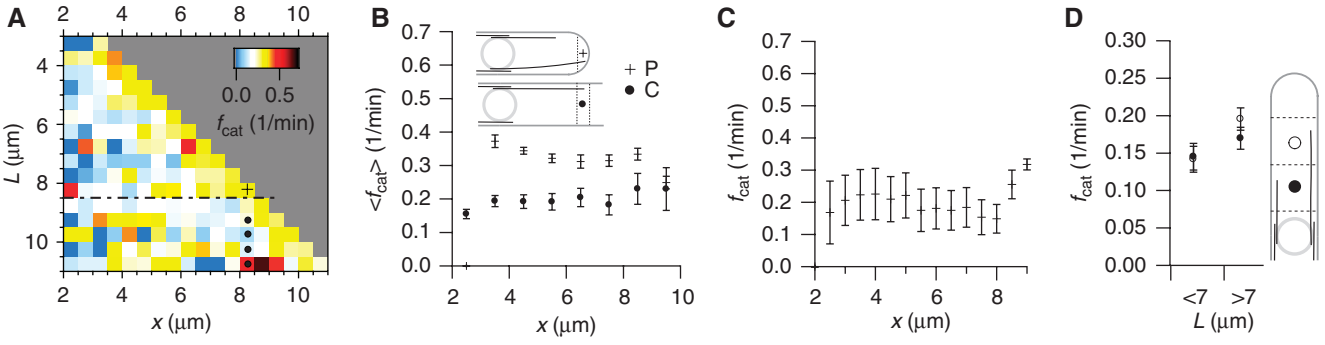

Figure 5 Spatially resolved f_{cat} measurements in *klp5Δklp6Δ* cells as a function of distance to the cell centre (x) in cells with different half lengths L. (**A**) $f_{cat}(x,L)$. The cross and circles refer for one specific x to the presentation of the data in (B). Statistics: N_{cat}=4797; N_{cells}=377; see also Supplementary Figure S2. (**B**) Crosses: f_{cat} at the poles of cells of different lengths (x=L). Circles: f_{cat} in the cytoplasm at position x, averaged over all cells with $L > x + 1$ μm. (**C**) $f_{cat}(x)$ for cells with L=9 ± 0.5 μm, corresponding to the dashed horizontal line in (B). (**D**) Average f_{cat} in cytoplasmic regions proximal and distal to the cell centre, for cells with normal (L<7 μm) and elongated (L>7 μm) sizes; see also Figure 2D. Statistics: L<7 μm: N_{cat}=117; N_{cells}=241; L>7 μm: N_{cat}=245; N_{cells}=173.

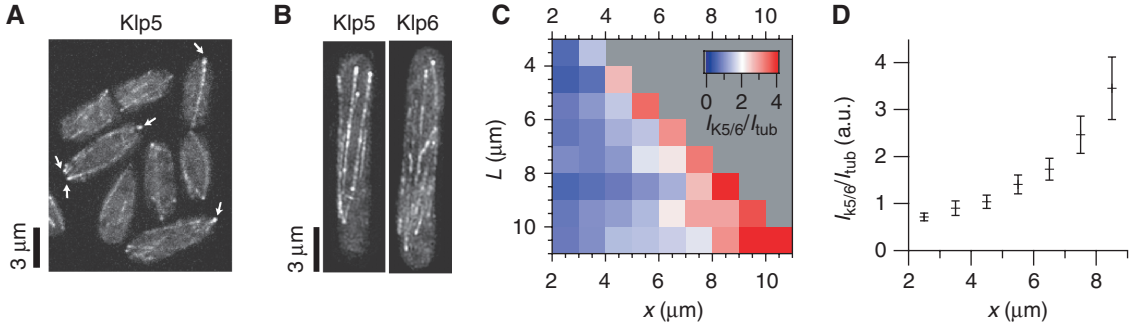

Figure 6 Spatially resolved measurements of the distribution of Klp5/6 on MT bundles. (**A**) *z*-maximum projections of untreated cells expressing Klp5-GFP. Arrows point out instances of high intensities within the cell pole regions. (**B**) *z*-maximum projections of elongated (HU-treated) cells expressing Klp5-GFP (left panel), or Klp6-GFP (right panel). (**C**) Average Klp5-GFP and Klp6-GFP intensity ($I_{K5/6}$) divided by average GFP-tubulin intensity (I_{tub}) as a function of intracellular position for different cell lengths (see also Supplementary Figure S5). (**D**) Same data as in (C) shown for $L=9\pm0.5$ µm (error bars are computed using the s.e.m. for $I_{Klp5/6}$ ($N_{cells}=52$) and for I_{tub} ($N_{cells}=37$) and the laws of error propagation for the ratio).

that were at the cell poles (Figure 6A). In addition, in elongated cells, we also observed high Klp5/6-GFP intensities on the tips of MTs that were not yet at cell poles (Figure 6B). To quantify this and to normalise for the fact that the tubulin polymer density (i.e. potential Klp5/6-GFP-binding sites) is higher in the cell centre, we measured ratios of average local Klp5/6-GFP intensities and average local GFP-bundle intensities (Figure 6C and D; see also Supplementary Figure S5). Corroborating the impression of visual inspections, this analysis indicated that there is more Klp5/6-GFP on MTs that are further away from the cell centre, with the highest intensity for MTs closest to the cell poles.

Discussion

Force generation and the modulation of MT dynamics at cell poles

On performing quantitative *in vivo* measurements, we find with high statistical significance that both the catastrophe frequency f_{cat} and the growth velocity v_g of MT bundle tips near the pole of interphase fission yeast cells are different from the dynamics in the cytoplasmic region in a way that depends on whether the opposite bundle tip resides near the other cell pole or not (Figure 4A–E). We think the easiest explanation for these observations would be the following: the growth of a bundle tip against the cell pole generates pushing forces, which lead to compressive forces on the MT, which in turn cause a reduction in growth velocity because addition of new tubulin subunits to the MT tip is physically hindered (Peskin *et al*, 1993; Mogilner and Oster, 1999; Doorn *et al*, 2000). *In vitro* experiments have shown that compressive polymerisation forces that build up when MTs grow against microfabricated walls reduce MT growth velocities by similar factors as we observe here *in vivo* (Dogterom and Yurke, 1997; Janson and Dogterom, 2004). *In vitro* measurements have also shown that low growth velocities tend to correspond to high values of f_{cat}, again in a manner that is quantitatively similar to our observations (Walker *et al*, 1988; Janson *et al*, 2003).

The build-up of compressive forces is expected to be strongest when bundle tips are simultaneously in contact with opposite cell poles (the P_P situation), and is expected to be stronger for short MTs than for long MTs (Dogterom and Yurke, 1997; Janson and Dogterom, 2004). This last effect would explain why the increase in f_{cat} at the cell poles is stronger in short cells than in long cells (Figures 2B and 5B). The presence of pushing forces that lead to motion of the central MT overlap zone away from the cell pole (Tran *et al*, 2001; Daga *et al*, 2006b) would also explain the increase in the velocity at which the opposite bundle tip moves through the cytoplasmic region in the C_P versus C_C situation (Figure 4E; note that the increase in velocity need not be identical to the MT growth velocity at the pole due to bending effects). In addition, the observed angle dependence of MT growth velocities and catastrophe rates appears to fit into this mechanical picture (Figure 4F–H). MTs growing through the cytoplasmic region do not experience any growth opposing forces (and therefore remain mostly straight) as long as they are able to elongate towards the cell pole. This is independent of whether there is contact with the cell membrane or not, as long as MT tips are able to freely slide along the cortex. Freely sliding tips may slightly bend due to lateral forces on the MT tip, but these forces are directed perpendicular to the growth direction and are therefore not expected to affect the growth velocity. Only when further sliding is prevented upon reaching the (extreme) cell pole, compressive forces build up and MTs start to seriously bend. Given the shape of the fission yeast cell, strong MT bending correlates on average with large contact angles (see e.g. Figure 4A). Already in the P_C situation, the nuclear anchoring of MTs can be sufficient to support the build-up of significant forces (see also Supplementary Figure S9). However, the observation that angles are on average larger in the P_P than in the P_C situation is consistent with the idea that compressive forces are largest in the former case.

Although force-induced effects may explain the pole-specific f_{cat} enhancement we observe in our experiments, it is important to note that this does not rule out a possible additional role for specific MT interacting proteins. General differences in MT growth dynamics between the cell pole and the cytoplasmic region, as have been observed by others before (Drummond and Cross, 2000; Tran *et al*, 2001; Grallert *et al*, 2006), may also be explained by (yet unknown) biochemical factors that are selectively located to either of these regions.

The role of Klp5/6 in MT length-dependent f_{cat} regulation

Our data indicate that there also exists a long-range regulation of f_{cat} in the cytoplasmic region, several micrometres away from the cell pole. This long-range regulation is diminished in strains where the kinesin-8 proteins Klp5/6 are deleted (Figures 2 and 5). We provide evidence that the density of Klp5/6 on MTs is highest near the plus tips of long MTs (Figure 6). As Klp5/6 are members of the kinesin-8 family, this non-uniform distribution is likely to be caused by plus-tip-directed motility (Pereira *et al*, 1997; Rischitor *et al*, 2004; Gupta *et al*, 2006; Varga *et al*, 2006; Mayr *et al*, 2007) (see also Supplementary Figure S5C and D where we show, for individual cases, motion of Klp5/6-GFP molecules along the MT lattice as well as the gradual increase in Klp5/6 intensity at a growing MT tip). These observations are in line with recent *in vitro* measurements on the budding yeast kinesin-8 protein Kip3, showing an increased density near the plus tips of long MTs (Varga *et al*, 2006). *In vitro*, it has also been shown that the kinesin-8 proteins Kip3 (*Saccharomyces cerevisiae*) and Kif18A (*Homo sapiens*) depolymerise longer GMPCPP-stabilised MTs faster than shorter ones (Varga *et al*, 2006; Mayr *et al*, 2007). On first glance, this may seem different to our findings, because we find no evidence that Klp5/6 would increase the MT depolymerisation velocity *in vivo*. However, dynamic MTs have an intrinsic tendency to depolymerise after a catastrophe event, which is different from the slow protein-driven depolymerisation observed for GMPCPP-stabilised MTs (Varga *et al*, 2006; Mayr *et al*, 2007). The effect of kinesin-8 proteins on dynamic MTs *in vivo* could thus be to promote catastrophes preferentially of long MTs, possibly by driving depolymerisation of a stabilising structure at the MT tip (Desai and Mitchison, 1997).

Interestingly, Daga *et al* (2006b) observed in fission yeast cells with an artificially displaced nucleus that MTs that were in the longer cell half underwent catastrophes more frequently than in the shorter cell half. We think these observations may be explained by an increase in f_{cat} with MT length. An increase in f_{cat} with MT length, but no length dependence of growth and shrinkage velocities also matches findings in mitotic *Xenopus* extracts (Dogterom *et al*, 1996), suggesting that there may be a similar mechanism in place.

In addition to the Klp5/6-dependent long-range regulation of f_{cat} in the cytoplasmic region, we also observe a strong decrease in f_{cat} at cell poles upon Klp5/6 deletion (compare upper traces in Figures 2B and 5B). This could (partly) be explained by the fact that MTs at cell poles are in fact the longest in a given cell. This is consistent with the fact that the decrease in f_{cat} at cell poles upon Klp5/6 deletion is more pronounced in longer cells (compare Figures 2B and 5B). However, we also find evidence that the density of Klp5/6 on MT tips is particularly high at cell poles even when compared with MTs of the same length in longer cells (see Figure 6A–C). We therefore think it is possible that Klp5/6 additionally accumulate at MTs that are at the cell pole and thus specifically contribute to a f_{cat} enhancement at cell poles. Interestingly, Gupta *et al* (2006) similarly reported that deletion of the Klp5/Klp6 homologue Kip3 in budding yeast lowered f_{cat} at the cell periphery more than in the cell centre.

Finally, we would like to point out that changes in MT dynamics in Klp5/6 deletion cells may in addition be caused by indirect (secondary) system responses. For instance, due to the reduced f_{cat} one expects more tubulin to be bound in polymer form and it could thus be that the slight ($\sim$15%) reduction in MT growth velocity in Klp5/6 deletion cells is a response to a lower concentration of free tubulin. Also, as f_{cat} is generally lower, there could on average be more MTs at cell poles. This could lead to lowering of the (shared) compressive forces on individual MTs, for example in the P_C situation, leading to a diminished force-induced increase in f_{cat} at cell poles.

Relevance of spatial regulation of f_{cat} in interphase fission yeast cells

We present evidence for two kinds of spatial regulation of MT dynamics in interphase fission yeast: (i) a local decrease in the growth velocity and a local enhancement of f_{cat} at cell poles and (ii) a long-range increase in f_{cat} with distance to the cell centre. The local regulation at cell poles provides clear functional advantages for MT-mediated transport of cell growth-promoting factors such as Tea1 (Mata and Nurse, 1997). Such transport requires that MTs reliably reach and undergo catastrophes at the cell poles; when MTs either undergo premature catastrophes or do not cease growth at cell poles, Tea1 transport and cell shape control are perturbed (Beinhauer *et al*, 1997; Mata and Nurse, 1997; Browning *et al*, 2000; Brunner and Nurse, 2000; Hayles and Nurse, 2001; Feierbach *et al*, 2004; Sawin and Snaith, 2004; Castagnetti *et al*, 2007). In addition, there is evidence that a second function of MTs in interphase fission yeast is to dynamically centre the nucleus by creating pushing forces at the cell poles (Tran *et al*, 2001; Tolic-Norrelykke *et al*, 2005). This mechanism benefits from long-range catastrophe regulation where long MTs undergo more catastrophes, because, in cells with displaced nucleus, fewer MTs reach the distal pole (due to premature catastrophes) and spend less time at the distal pole (due to the relatively high f_{cat}). Thus, the asymmetry of the pushing forces is enhanced and nuclear centring is accelerated (see accompanying paper by Föthke *et al*, 2009).

Relevance of our measurements to other systems

In addition to the situation in the fission yeast system, it is interesting to note that f_{cat} is also enhanced at the boundaries of animal cells (Komarova *et al*, 2002; Mimori-Kiyosue *et al*, 2005) by a yet unknown mechanism. Our findings in fission yeast, taken together with earlier *in vitro* observations (Dogterom and Yurke, 1997; Janson *et al*, 2003; Janson and Dogterom, 2004), suggest that there are intrinsic relations between polymerisation force, v_g, and f_{cat} that help terminate MT growth at physical boundaries.

In a living cell, the spatial extent of the cell and the length of its MT cytoskeleton must be well adapted to each other. There has been evidence that MT dynamics play a role in establishing cell shape (Kirschner and Mitchison, 1986; Hayles and Nurse, 2001). Our data indicate that, vice versa, the shape of a cell also influences MT dynamics. Thus, cell shape and MT organisation may not be separable components but should be viewed as one system.

Klp5/Klp6 are part of the kinesin-8 family, comprising Kip3 (*S. cerevisiae*), KLP67A (*Drosophila melanogaster*), Kif18A (*H. sapiens*) and KipB (*Aspergillus nidulans*), which have in common that mutants show defects in mitosis (Garcia *et al*, 2002; West *et al*, 2002; Rischitor *et al*, 2004; Tytell and Sorger, 2006; Mayr *et al*, 2007; Stumpff *et al*, 2008). In this context, it has been speculated that a kinesin-8-mediated increase in f_{cat} with MT length could contribute to proper chromosome centring and spindle length regulation (Gardner *et al*, 2008; Stumpff *et al*, 2008). As discussed above, our data provide good experimental evidence that kinesin-8 proteins indeed specifically enhance f_{cat} of long MTs.

Conclusions

Our data suggest that MT polymerisation forces produced at fission yeast cell poles reduce MT growth velocities and enhance the probability that MTs undergo catastrophes. Moreover, we present evidence that kinesin-8 proteins enhance the f_{cat} of long MTs. Both mechanisms contribute to a robust termination of MT growth at fission yeast cell poles without compromising growth through the cytoplasm. These discoveries were strongly facilitated by the development of automated image analysis procedures, which made it possible to obtain the statistics that are necessary to study the apparently stochastic processes of MT catastrophes. We would like to stress that regulation of MT dynamics in fission yeast is probably not only mediated by mechanical forces and kinesin-8 proteins but also by other regulatory proteins (e.g. Tip1, Tea1, Mal3 or Peg1; Mata and Nurse, 1997; Brunner and Nurse, 2000; Busch and Brunner, 2004; Grallert *et al*, 2006). Further systematic and quantitative studies will be necessary to fully uncover the complex interplay between mechanical and biochemical regulation of MT dynamics in fission yeast and other eukaryotic systems.

Materials and methods

Cell culturing

S. pombe cells were grown using standard conditions (Moreno *et al*, 1991). Cells expressing GFP-α2-tubulin from a single, exogenously integrated locus under the control of the nmt1 promoter, were grown in Edinburgh minimal medium supplemented with 15 μM thiamine. For *klp5/6* deletion experiments we constructed a strain where both the *klp5* and *klp6* genes were deleted and GFP-α2-tubulin was expressed as above. These cells were also grown in Edinburgh minimal medium supplemented with 15 μM thiamine. Cells expressing Klp5-GFP or Klp6-GFP were grown in yeast extract medium.

Strains used in this study

YY105: *leu1-32 ura4-d18 lys1+ ::nmt1-GFP-α2tub, h90* (Yamamoto *et al*, 1999)
DB1767: *klp5Δ::ura4+ klp6Δ::ura4+ lys1+ ::nmt1-GFP-α2tub ade6-M216 his3-D1 leu1-32 ura4-D18, h90* (this study)
McI 485: *klp5::GFP::ura4 ade6-M210 his3-D1 leu1-32 ura4-D18, h+* (West *et al*, 2001)
McI 486: *klp6::GFP::ura4 ade6-M210 his3-D1 leu1-32 ura4-D18, h−* (West *et al*, 2001).

Microscopy

Cells were mounted on agarose pads following protocols by Tran *et al* (2004) and imaged at 24–25°C with a confocal spinning disc microscope, comprising a confocal scanner unit (CSU22; Yokogawa Electric Corp.) attached to an inverted microscope (DMIRB; Leica) equipped with a ×100/1.3 NA oil immersion lens (PL FLUOTAR; Leica) and a built-in ×1.5 magnification changer lens. The sample was illuminated using a 488 nm laser (Sapphire 488-30; Coherent Inc.). Images were captured by an EM-CCD (C9100; Hamamatsu Photonics) controlled by software from VisiTech International. *z*-maximum projections were computed from stacks of about 20 images acquired with 125 ms exposure time at 0.3 μm *z*-spacing. For measurement of MT dynamics, 90 *z*-stacks were acquired with 8 s time delay between subsequent stacks, corresponding to 12 min observation time.

Image analysis

See Supplementary information.

Note added in proof

We would like to point out two recently published articles investigating the effect of Klp5/6 on MT dynamics both *in vivo* (Unsworth *et al*, 2008) and *in vitro* (Grissom *et al*, 2008). In the first article, measurements consistent with our observations are presented showing that the catastrophe frequency of MTs is suppressed in Klp5/6 deletion mutants. In the second article, the authors show that unlike kinesin-8 proteins such as Kip3, Klp5/6 proteins do not possess an MT depolymerisation activity *in vitro*. This suggests that Klp5/6 may induce catastrophes by a mechanism that is distinct from kinesin-8 proteins in other species.

Supplementary information

Supplementary information is available at the *Molecular Systems Biology* website (www.nature.com/msb).

Acknowledgements

This study is part of the research programme of the Stichting voor Fundamenteel Onderzoek der Materie (FOM), which is financially supported by the Nederlandse Organisatie voor Wetenschappelijk Onderzoek (NWO). We thank Dietrich Foethke and Francois Nedelec for many fruitful discussions. We thank Sander Tans and Bela Mulder for carefully reading the paper and Takashi Toda for kindly providing *klp5* and *klp6* deletion strains as well as Dick McIntosh for sharing Klp5/6-GFP strains. We gratefully acknowledge support from HSFP Research Grant RPG11/2005. CT was supported by a Marie Curie Fellowship.

Conflict of interest

The authors declare that they have no conflict of interest.

References

Beinhauer JD, Hagan IM, Hegemann JH, Fleig U (1997) Mal3, the fission yeast homologue of the human APC-interacting protein EB-1 is required for microtubule integrity and the maintenance of cell form. *J Cell Biol* **139:** 717–728

Browning H, Hayles J, Mata J, Aveline L, Nurse P, McIntosh JR (2000) Tea2p is a kinesin-like protein required to generate polarized growth in fission yeast. *J Cell Biol* **151:** 15–27

Brunner D, Nurse P (2000) CLIP170-like tip1p spatially organizes microtubular dynamics in fission yeast. *Cell* **102:** 695–704

Busch KE, Brunner D (2004) The microtubule plus end-tracking proteins mal3p and tip1p cooperate for cell-end targeting of interphase microtubules. *Curr Biol* **14:** 548–559

Carazo-Salas RE, Nurse P (2006) Self-organization of interphase microtubule arrays in fission yeast. *Nat Cell Biol* **8:** 1102–1107

Castagnetti S, Novak B, Nurse P (2007) Microtubules offset growth site from the cell centre in fission yeast. *J Cell Sci* **120:** 2205–2213

Daga RR, Lee KG, Bratman S, Salas-Pino S, Chang F (2006a) Self-organization of microtubule bundles in anucleate fission yeast cells. *Nat Cell Biol* **8:** 1108–1113

Daga RR, Yonetani A, Chang F (2006b) Asymmetric microtubule pushing forces in nuclear centering. *Curr Biol* **16:** 1544–1550

Desai A, Mitchison TJ (1997) Microtubule polymerization dynamics. *Annu Rev Cell Dev Biol* **13:** 83–117

Dogterom M, Felix M-A, Guet CC, Leibler S (1996) Influence of M-phase chromatin on the anisotropy of microtubule asters. *J Cell Biol* **133:** 125–140

Dogterom M, Kerssemakers JW, Romet-Lemonne G, Janson ME (2005) Force generation by dynamic microtubules. *Curr Op Cell Biol* **17:** 67–74

Dogterom M, Leibler S (1993) Physical aspects of the growth and regulation of microtubule structures. *Phys Rev Lett* **70:** 1347–1350

Dogterom M, Yurke B (1997) Measurement of the force–velocity relation for growing microtubules. *Science* **278:** 856–860

Doorn GSv, Tanase C, Mulder BM, Dogterom M (2000) On the stall force for growing microtubules. *Eur Biophys J* **29:** 2–6

Drummond DR, Cross RA (2000) Dynamics of interphase microtubules in *Schizosaccharomyces pombe*. *Curr Biol* **10:** 766–775

Feierbach B, Verde F, Chang F (2004) Regulation of a formin complex by the microtubule plus end protein tea1p. *J Cell Biol* **165:** 697–707

Föthke D, Makushok T, Brunner D, Nédélec F (2009) Force- and length-dependent catastrophe activities explain interphase microtubule organization in fission yeast. *Mol Syst Biol* **5:** 241

Garcia MA, Koonrugsa N, Toda T (2002) Two kinesin-like Kin I family proteins in fission yeast regulate the establishment of metaphase and the onset of anaphase A. *Curr Biol* **12:** 610–621

Gardner MK, Odde DJ, Bloom K (2008) Kinesin-8 molecular motors: putting the brakes on chromosome oscillations. *Trends Cell Biol* **18:** 307–310

Grallert A, Beuter C, Craven RA, Bagley S, Wilks D, Fleig U, Hagan IM (2006) *S. pombe* CLASP needs dynein, not EB1 or CLIP170, to induce microtubule instability and slows polymerization rates at cell tips in a dynein-dependent manner. *Genes Dev* **20:** 2421–2436

Grissom PM, Fiedler TA, Grishchuk EL, Nicastro D, West RR, McIntosh JR (2008) Kinesin-8 from fission yeast: a heterodimeric, plus end-directed motor that can couple microtubule depolymerization to cargo movement. *Mol Biol Cell* (e-pub ahead of print, November 2008)

Gupta ML, Carvalho P, Roof DM, Pellman D (2006) Plus end-specific depolymerase activity of Kip3, a kinesin-8 protein, explains its role in positioning the yeast mitotic spindle. *Nat Cell Biol* **8:** 913–923

Hagan IM (1998) The fission yeast microtubule cytoskeleton. *J Cell Sci* **111:** 1603–1612

Hayles J, Nurse P (2001) A journey into space. *Nat Rev Mol Cell Biol* **2:** 647–656

Hoog JL, Schwartz C, Noon AT, O'Toole ET, Mastronarde DN, McIntosh JR, Antony C (2007) Organization of interphase microtubules in fission yeast analyzed by electron tomography. *Dev Cell* **12:** 349–361

Howard J, Hyman AA (2007) Microtubule polymerases and depolymerases. *Curr Opin Cell Biol* **19:** 31–35

Howell B, Odde DJ, Cassimeris L (1997) Kinase and phosphatase inhibitors cause rapid alterations in microtubule dynamic instability in living cells. *Cell Mot Cytoskeleton* **38:** 201–214

Inoue S, Salmon ED (1995) Force generation by microtubule assembly disassembly in mitosis and related movements. *Mol Biol Cell* **6:** 1619–1640

Janson ME, Dogterom M (2004) Scaling of microtubule force–velocity curves obtained at different tubulin concentrations. *Phys Rev Lett* **92:** 248101–248104

Janson ME, Dood MEd, Dogterom M (2003) Dynamic instability of microtubules is regulated by force. *J Cell Biol* **161:** 1029–1034

Kirschner M, Mitchison T (1986) Beyond self-assembly: from microtubules to morphogenesis. *Cell* **45:** 329–342

Komarova YA, Vorobjev IA, Borisy GG (2002) Life cycle of MTs: persistent growth in the cell interior, asymmetric transition frequencies and effects of the cell boundary. *J Cell Sci* **115:** 3527–3539

Mata J, Nurse P (1997) Tea1 and the microtubular cytoskeleton are important for generating global spatial order within the fission yeast cell. *Cell* **89:** 939–949

Mayr MI, Hummer S, Bormann J, Gruner T, Adio S, Woehlke G, Mayer TU (2007) The human kinesin Kif18A is a motile microtubule depolymerase essential for chromosome congression. *Curr Biol* **17:** 488–498

Mimori-Kiyosue Y, Grigoriev I, Lansbergen G, Sasaki H, Matsui C, Severin F, Galjart N, Grosveld F, Vorobjev I, Tsukita S, Akhmanova A (2005) CLASP1 and CLASP2 bind to EB1 and regulate microtubule plus-end dynamics at the cell cortex. *J Cell Biol* **168:** 141–153

Mitchison J, Kirschner M (1984) Dynamic instability of microtubule growth. *Nature* **312:** 237–242

Mogilner A, Oster G (1999) The polymerization ratchet model explains the force–velocity relation for growing microtubules. *Eur Biophys J* **28:** 235–242

Moreno S, Klar A, Nurse P (1991) Molecular genetic analysis of fission yeast *Schizosaccharomyces pombe*. *Methods Enzymol* **194:** 795–823

Niethammer P, Bastiaens P, Karsenti E (2004) Stathmin–tubulin interaction gradients in motile and mitotic cells. *Science* **303:** 1862–1866

Odde DJ (1995) Kinetics of microtubule catastrophe assessed by probabilistic analysis. *Biophys J* **69:** 796–802

Pereira AJ, Dalby B, Stewart RJ, Doxsey SJ, Goldstein LSB (1997) Mitochondrial association of a plus end-directed microtubule motor expressed during mitosis in *Drosophila*. *J Cell Biol* **136:** 1081–1090

Peskin CS, Odell GM, Oster GF (1993) Cellular motions and thermal fluctuations—the Brownian ratchet. *Biophys J* **65:** 316–324

Rischitor PE, Konzack S, Fischer R (2004) The Kip3-like kinesin KipB moves along microtubules and determines spindle position during synchronized mitoses in *Aspergillus nidulans* hyphae. *Eukaryot Cell* **3:** 632–645

Sawin KE, Snaith HA (2004) Role of microtubules and tea1p in establishment and maintenance of fission yeast cell polarity. *J Cell Sci* **117:** 689–700

Stumpff J, von Dassow G, Wagenbach M, Asbury C, Wordeman L (2008) The kinesin-8 motor Kif18A suppresses kinetochore movements to control mitotic chromosome alignment. *Dev Cell* **14:** 252–262

Sveiczer A, Novak B, Mitchison JM (1996) The size control of fission yeast revisited. *J Cell Sci* **109:** 2947–2957

Tolic-Norrelykke IM, Sacconi L, Stringari C, Raabe I, Pavone FS (2005) Nuclear and division-plane positioning revealed by optical micromanipulation. *Curr Biol* **15:** 1212–1216

Tran PT, Marsh L, Doye V, Inoue S, Chang F (2001) A mechanism for nuclear positioning in fission yeast based on microtubule pushing. *J Cell Biol* **153:** 397–411

Tran PT, Paoletti A, Chang F (2004) Imaging green fluorescent protein fusions in living fission yeast cells. *Methods* **33:** 220–225

Tytell JD, Sorger PK (2006) Analysis of kinesin motor function at budding yeast kinetochores. *J Cell Biol* **172:** 861–874

Unsworth A, Masuda H, Dhut S, Toda T (2008) Fission yeast kinesin-8 Klp5 and Klp6 are interdependent for mitotic nuclear retention and required for proper microtubule dynamics. *Mol Biol Cell* **19:** 5104–5115

Varga V, Helenius J, Tanaka K, Hyman AA, Tanaka TU, Howard J (2006) Yeast kinesin-8 depolymerizes microtubules in a length-dependent manner. *Nat Cell Biol* **8:** 957–962

Verde F, Dogterom M, Stelzer E, Karsenti E, Leibler S (1992) Control of microtubule dynamics and length by cyclin A- and cyclin B-dependent kinases in *Xenopus* egg extracts. *J Cell Biol* **118:** 1097–1108

Walker RA, Obrien ET, Pryer NK, Soboeiro MF, Voter WA, Erickson HP, Salmon ED (1988) Dynamic instability of individual microtubules analyzed by video light-microscopy—rate constants and transition frequencies. *J Cell Biol* **107:** 1437–1448

West RR, Malmstrom T, McIntosh JR (2002) Kinesins klp5(+) and klp6(+) are required for normal chromosome movement in mitosis. *J Cell Sci* **115:** 931–940

West RR, Malmstrom T, Troxell CL, McIntosh JR (2001) Two related kinesins, klp5(+) and klp6(+), foster microtubule disassembly and are required for meiosis in fission yeast. *Mol Biol Cell* **12:** 3919–3932

Yamamoto A, West RR, McIntosh JR, Hiraoka Y (1999) A cytoplasmic dynein heavy chain is required for oscillatory nuclear movement of meiotic prophase and efficient meiotic recombination in fission yeast. *J Cell Biol* **145:** 1233–1249

Zheng LF, Schwartz C, Wee LM, Oliferenko S (2006) The fission yeast transforming acidic coiled coil-related protein Mia1p/Alp7p is required for formation and maintenance of persistent microtubule-organizing centers at the nuclear envelope. *Mol Biol Cell* **17:** 2212–2222

SUPPLEMENTAL INFORMATION

Force- and Klp5/6-dependent effects in the spatial dependence of fission yeast microtubule dynamics

Christian Tischer, Damian Brunner, and Marileen Dogterom

Table of Contents:

Automated spatially resolved f_{cat} measurements.

In order to measure f_{cat} in an unbiased way and with the necessary statistics we developed computer algorithms for automated detection of bundle catastrophes and bundle tips from the acquired confocal image stacks. Here, we provide an overview of the processing steps, which are described in more detail elsewhere (Tischer *et al*, in press). The source code of the processing software is available upon request. We first performed a 3-D Gaussian averaging on each z-stack to decrease imaging noise. To reduce data complexity we then calculated z-maximum projections of each stack, resulting in a 2-D time-series. Next, we reduced blur by 2-D de-convolution of each image with the microscope's point spread function. Finally, we decreased noise by an edge preserving Kuwahara filter (M. Kuwahara *et al*, 1976; P. Bakker *et al*, 1999) that we modified specifically for linear structures such as microtubules. Overall, we found that this sequence of filtering steps reduced imaging noise significantly while preserving edges and intensity values very well (Fig. S1A). In order to detect bundle tips the software first computes threshold intensity images (Fig. S1A). The software then assigns to each pixel the z-plane in which the corresponding maximum intensity value was found during the z-maximum projection. Multiplying the z-plane number with the distance between z-planes (i.e. 0.3 μm) yields the z-position of the respective microtubule part (Fig. S1A). Next, the software determines the orientation of the bundle axis, allowing it to compute the derivative of the intensity along the bundles (Fig. S1A). The derivative is particularly high at the end of the bundle, where fluorescence drops to the cellular background level (Fig. S1A). Thresholding of the resulting derivative image thus yields the location of bundle tips (Fig. S1A). To obtain local microtubule dwell times, the number of detected growing bundle tips is multiplied with 8 seconds as this is the time-interval between successive image stacks.

The detection of microtubule catastrophes is based on analysis of difference images (DIs, Fig. S1B&C), which is a standard method for motion detection in movies. This method was for example used previously to aid visual detection of microtubule motions inside cells (Komarova

et al, 2002). We fully automated the detection of microtubule shrinkage events in these DIs. The algorithm automatically identifies extended regions of significant fluorescence loss, as occurring between subsequent images (extended dark regions in Figure S1C). For this, the algorithm only considers pixels where the loss of intensity is above the noise level ("noise" is due to photon counting statistics but also due to diffusion of free tubulin inside the cell). To eliminate events where local fluorescence loss is due to sideward translocation of microtubules rather than shrinkage, the neighborhood of the region is scanned for a fluorescence gain region of similar shape, which appears if translocation were taking place (Fig. S1D contains examples of such translocation events). Only if *no* such complementary region is present the fluorescence loss is assigned to a shrinkage event (Fig. S1D).

At our temporal resolution, the depolymerization of a whole microtubule typically shows up as a sequence of shrinkage events in successive DIs. The actual time and position of the catastrophe is however only determined by the onset of shrinkage. Thus, the first shrinkage event needs to be found. As can be seen in Figure S1BC, the algorithm operates on DIs calculated between every second image in the movie. Thus, shrinkage events in successive DIs contain overlapping information. This allows the algorithm to test whether a shrinkage event overlaps with a shrinkage event in the preceding DI. Only if this is *not* the case the shrinkage event is assigned to a catastrophe. Finally, only catastrophes where a corresponding bundle tip was identified in the same image are counted as bundle catastrophes.

In general, events less than 1.5 μm away from the cell center were not taken into account (boxed area in Fig. S1D), because it is difficult to reliably detect catastrophes of short microtubules in the crowded cell center region.

Accuracy of the automated f_{cat} measurements.

The above algorithm contains a number of steps in which one has to set a threshold level above which events are accepted as significant and below which they are regarded to be within the

noise level. Setting these threshold levels allows one to minimize the total of false-positive and false-negative events (high thresholds yield relatively few false-positives but more false-negatives and vice versa).

We tested the algorithm's performance by comparing its automated assignments with visual inspection in a random sample of 10 cells (corresponding to 2 hours total observation time). We on purpose put the threshold for bundle tip detection rather high such that the algorithm misses about 15% of the bundle tips, but only detects 1% false-positives. The reason for this choice is that false-positive bundle tips would lead to a systematic underestimation of f_{cat}, because there are no corresponding catastrophes. On the other hand, missed bundle tips are no problem because the algorithm is programmed such that it only accepts catastrophes if the corresponding bundle tip was detected as well. For catastrophe detection, we chose threshold levels that lead to a balanced percentage of false-positives (~6%) and false-negatives (~5%). The spatial differences in f_{cat} that we discuss in the main text are all well beyond the error that this may introduce into our measurements.

Opposite bundle tip detection.

We also developed software that automatically detects whether the other end of a given bundle is at the opposite cell pole. For a given detected bundle tip ("Bundle Tips" in Figure S1A), the algorithm first determines the direction of the microtubule axis at the tip ("Orientation" in Figure S1A). The algorithm then follows the microtubule axis, constantly exploiting the "Orientation" information, till it reaches the point when proceeding further into the direction of "Orientation" is no more possible as there are no more pixels belonging to a microtubule; the latter is inferred from the "threshold" image (Figure S1A). Figure S4A schematically illustrates how the algorithm step-by-step proceeds along a microtubule bundle till it reaches its other end. If this procedure terminates within the opposite cell pole region (or opposite cytoplasm), the bundle tip is assigned as belonging to the classes P_P or C_P (or P_C or C_C), depending on its own

position. Of course, complicated situations can arise where it is not easy to follow a bundle, for example when two bundles are crossing. We programmed the algorithm such that ambiguous events of such kinds are not taken into account. This discards data but ensures a good accuracy of the assigned events. We tested the algorithm's performance by comparing its assignments with visual inspection in a random sample of 5 cells (corresponding to 1 hour total observation time). For both cases – with and without opposite contact – we found about 7% false-positives. The 7% wrong assignments slightly mask differences between the two classes. The effect that bundle presence at the opposite pole has on microtubule dynamics may thus be even slightly larger than shown in the main text.

Bundle growth and shrinkage velocities in the cytoplasm.

Bundle growth and shrinkage velocities in the cytoplasm were automatically determined from the same GFP-tubulin movies that were also used for the f_{cat} measurements. Shrinkage velocities were computed as $\Delta x/16s$, where Δx is the length of the detected fluorescence loss area; 16s is the time interval between images from which the difference images were computed (Fig. S1B-D). The growth velocity analysis was very similar, but instead of detecting areas of significant fluorescence loss, we programmed the algorithm to detect areas of significant fluorescence increase between every 3rd image (Δt=24s, Fig. S4B). Growth velocities were computed as $\Delta x/24s$, where Δx is the length of the detected fluorescence increase area. For both shrinkage and growth, only events that occurred at a bundle tip were taken into account. For shrinkage velocities we required in addition that a catastrophe had just occurred. This means that we measure velocities at the onset of shrinkage.

Bundle growth velocities at cell poles.

Bundle growth measurements at the cell pole are more difficult, because microtubule growth does not necessarily result in bundle tip displacement. To investigate whether opposite bundle contact would alter bundle growth we monitored GFP-tubulin speckle translocation using the same data sets as for the f_{cat} measurements. Whenever the algorithm detected the same bundle tip at the cell pole in two subsequent images, it calculated the cross-correlation (CC) between the intensity profile I(*r*) at the bundle tip at time t and at time t+8s in the next image (Figure S4C shows an example). The CC is given by:

$CC(dr) = (I_t(r)-m_t)\ (I_{t+8s}(r+dr)-m_{t+8s}) / (s_t\ s_{t+8s})$,

where m_t is the mean intensity of $I_t(r)$ and s_t is the standard deviation. The CC peaks at the displacement *dr* where both profiles match best. The microtubule growth speed is then given by *dr*/8s, which amounts in the example shown to 0.2µm/8s=1.5µm/min.

The 3-D distances dr_i between neighboring pixels in the bundle were computed according to dr_i=Sqrt*(dx_i^2+dy_i^2+dz_i^2);* the distance *r* between separated points in the bundle was computed as $\sum dr_i$, i.e. summing the 3-D path along the bundle axis.

Bundle angle with cellular axis.

Given the mechanical boundary conditions imposed by the fission yeast cell wall and the nucleus, the angle that the leading part of a bundle encloses with the long axis of the cell can be taken as a measure of MT bending. To determine this angle we took the 3-D position of the bundle tip (xb_0,yb_0,zb_0) and of a second point (xb_1,yb_1,zb_1) that was about 770 nm behind the bundle tip (about 7 pixels of 110 nm within the imaging plane). From these coordinates we computed the vector $\mathbf{r_b}$=(xb_1-xb_0, yb_1-yb_0, zb_1-zb_0)**,** which lies approximately parallel to the leading part of the bundle. For each cell, the software also determined a vector $\mathbf{r_c}$ pointing along the long axis of the cell (not shown). The angle α that the leading part of the bundle encloses with the cellular axis was then computed as $\alpha' = \frac{180}{\pi}\arccos\left(\frac{\vec{r}_b\vec{r}_c}{|\vec{r}_b||\vec{r}_c|}\right)$ and $\alpha = \min(\alpha', 180-\alpha')$.

Spatially resolved Klp5-GFP, Klp6-GFP, and GFP-tubulin intensity measurements.

In z-maximum projections of image stacks of the respective strain, we (automatically) determined pixels whose intensity (i_{pixel}) was 2-fold brighter than the average cellular background (i_{bg}). For all three strains (Klp5-GFP, Klp6-GFP, and GFP-tubulin) this simple procedure reliably selected pixels that appeared to be along elongated structures (Fig. S5A&B). The intensity in each selected pixel was then normalized according to $i_{norm}=(i_{pixel}-i_{bg})$ and the sum of all selected pixels in a given range of X was computed as $I_{norm}(X) = \sum i_{norm}$. Values of $I_{norm}(X)$ were computed in N different cells and an average was computed as $\langle I_{norm}(X)\rangle = 1/N \sum I_{norm}(X)$. For GFP-tubulin these values ($I_{tub} = \langle I_{norm}(X)\rangle$) roughly correspond to the local tubulin polymer mass, and for Klp5/6-GFP these values ($I_{klp5/6} = \langle I_{norm}(X)\rangle$) roughly correspond to the local density of Klp5/6-GFP accumulations that are sufficiently dense (bright) to be selected by the requirement $i_{pixel}>2\ i_{bg}$. Figure 6C in the main text shows the ratio of $I_{klp5/6}$ and I_{tub}.

Examples of Klp5/6 dynamics

In general, the dynamic behavior of Klp5/6-GFP was very difficult to image, because the MTs appeared to be rather densely covered with Klp5/6 proteins, and because the signals were subject to photo-bleaching. This prevented us from a systematic quantitative analysis of Klp5/6 dynamics, but Figures S5C&D do show a few examples of the type of dynamics we observe. In Figure S5C one can see indications of particles moving along the MT lattice towards the MT tips at a speed of roughly 3 μm/min, indicating that Klp5/6 molecules behave, as expected, as plus-end directed MT motors. Figure S5D shows an example where the intensity of Klp5/6-GFP on growing bundle tips increases over time. This intensity decreases again once the MT starts shrinking.

Hydroxyurea treatment

For some experiments, cells were treated with hydroxyurea (HU) to obtain lengthy cells. We chose not to use temperature sensitive cell cycle mutants as temperature shifts affect microtubule dynamics. We looked for conditions where HU treatment would yield longer cells, but would not alter microtubule dynamics. Treating cells for 3-9h with a commonly used concentration of 11mM HU efficiently extended the cell size range (compare Fig. S6A&B), but also significantly reduced the average f_{cat} (untreated: 0.46±0.1 min^{-1}; treated: 0.24±0.1 min^{-1}). We thus investigated whether lower HU concentrations would affect microtubule dynamics less. Indeed, administrating 3mM HU for 3-9 h did not significantly alter the average f_{cat}, as evaluated in cells of half lengths between 5 and 7 micrometer (untreated: 0.46±0.1 min^{-1}; treated: 0.45±0.1 min^{-1}). Using this low dose of 3mM did not completely block the cell cycle but resulted in a population of cells dividing at sufficiently increased length (Figs. S6C&D). This allowed us to test the effect of prolonged HU treatment. We found that 3mM HU did not detectably alter the average f_{cat} even after treatment for 15-24h (untreated: 0.46±0.1 min^{-1}; treated: 0.46±0.1 min^{-1}), which excludes possible secondary effects caused by accumulation of errors in DNA replication. In addition we found that 3-24h treatments with 3mM HU also hardly altered average cytoplasmic microtubule growth (v_g) and shrinkage (v_s) velocities (untreated: v_g=2.41±0.02μm/min, v_s=8.3±0.1μm/min; treated: v_g=2.39±0.02μm/min, v_s=8.7 ±0.12μm/min).

Additional analyses of MT dynamics close to cell poles

In order to test more carefully from which distance to the cell pole force related effects begin to play a role, we performed several additional analyses as presented in this section. From visual inspection of movies with GFP stained MTs it appears that MTs elongate quite freely until they get mechanically stuck in the very tip of the cell pole. Figure S7A shows the velocity at which bundle tips move towards the cell pole as a function of distance to the cell pole (dxPole). We indeed find a reduction in growth velocity only when bundle tips are closer than 1 μm to the cell pole (see also Figure 3C in the main text). Moreover, we extended the analysis shown in Figures

3B&C and systematically analyzed bundle tips at different distances to the cell pole (in the main text we only distinguish the two regions: “Pole” and “Cytoplasmic”). We only find a significant effect of the position of the opposite bundle tip for MTs whose tips are closer than 0.5 μm to the cell pole (Figure S7B). Finally, we computed the angle dependence of f_{cat} for bundle tips whose distance to the cell pole are within 0.5-1 μm. In contrast to the bundle tips that are within 0-0.5 μm distance to the cell pole, we find in this case no significant angle dependence of f_{cat} (Figure S7C). This result suggests that MT orientation only begins to affect f_{cat} when the MT tips are very close to the cell pole. Summarizing, the results in Figures S7A-C indicate that force-related effects only play a significant role for MTs that are closer than 1 μm (and possibly 0.5 μm) to the cell pole.

To further confirm this, we plotted the average f_{cat} of MTs that are at a certain distance from the cell center (see lower trace in Figure 2B), excluding events that were less than either 1, 2, or 3 μm away from the cell pole (see Figure S7D). In all cases, there is a significant increase of f_{cat} with distance to cell center, indicating that this increase is not due to “contamination” of the data with “cell pole related” effects.

SUPPLEMENTAL REFERENCES

Komarova YA, Vorobjev IA, Borisy GG (2002) Life cycle of MTs: persistent growth in the cell interior, asymmetric transition frequencies and effects of the cell boundary. *J Cell Sci* **115:** 3527-3539.

M. Kuwahara, K. Hachimura, S. Eiho, Kinoshita M (1976) *Digital Processing of Biomedical Images (Plenum Press, New York)***:** 187-203.

P. Bakker, L.J. Van Vliet, Verbeek PW (1999) Edge Preserving Orientation Adaptive Filtering *IEEE Computer Society Conference on Computer Vision and Pattern Recognition* **1**.

Tischer C, Brunner D, Dogterom M (in press) Biophysical Tools for Biologists, Volume 2: Methods In Vivo. *Methods in Cell Biology*.

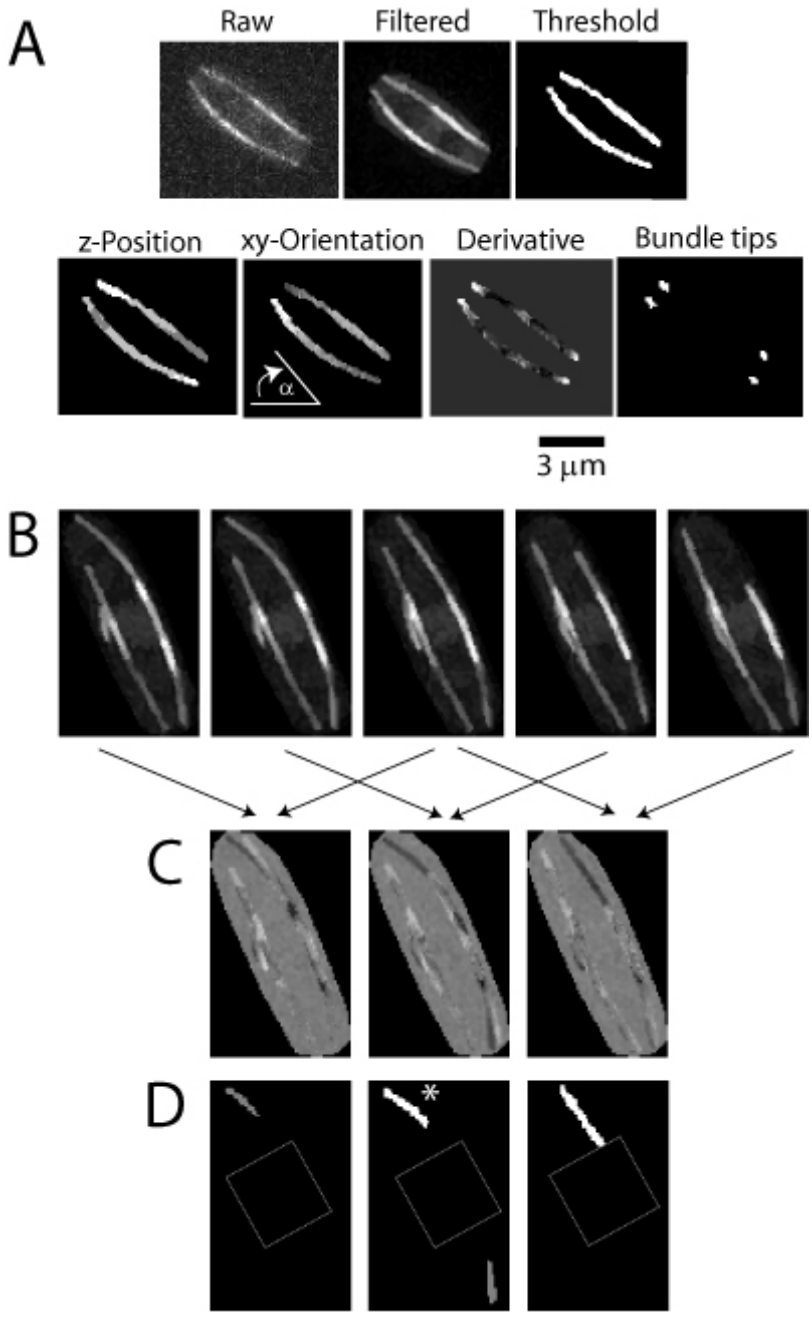

Figure S1 Automated catastrophe frequency measurements. **A)** Panels showing the steps involved in detection of bundle tips and orientation. Raw: z-maximum projection of a 3D stack of fluorescence images of a GFP-tubulin expressing fission yeast cell. Filtered: same image after application of filtering steps. Threshold: white pixels are assigned as being part of a microtubule bundle. z-Position: linear gray scale indicating z-position of the respective pixel. xy-Orientation: linear gray scale indicating bundle orientations between α =60 degrees (white) and α =0 degrees (black). Derivative: directional derivatives of the intensity image along the bundle orientations. Bright pixels correspond to high derivatives. Bundle tips: threshold of the derivative image, yielding the final bundle tip assignment. **B)** Image sequence with a time delay of 8s. **C)** Difference images computed from images in B as indicated by the arrows. Bright (dark) areas correspond to gain (loss) of fluorescence intensity. **D)** Motion label images; white (grey) areas denote automatically assigned shrinkage (translocation) events. The star indicates a shrinkage event corresponding to a catastrophe. The dotted box denotes the cell center (nuclear) region, which was not included in our analyses.

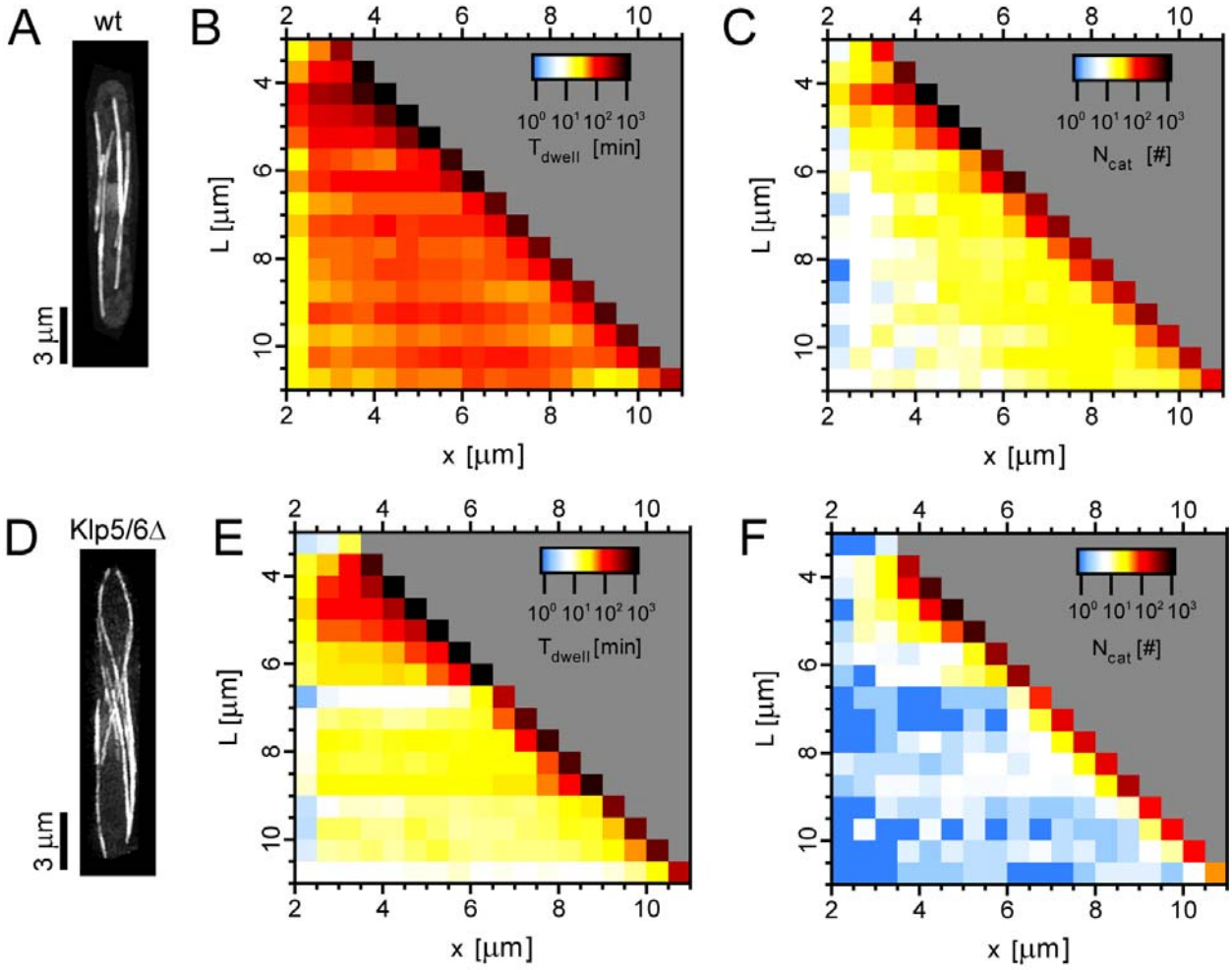

Figure S2 Example images of MTs in wild-type and *klp5*Δ*klp6*Δ cells and statistics for spatially resolved f_{cat} measurements. **A)** GFP-tubulin z-maximum projection in an elongated (hydroxyurea treated) wild-type cell. **B)** Time for which growing bundle tips were monitored and **C)** number of catastrophes observed in wild-type cells (note the log-scale: e.g. 3 corresponds to 1000) **D)** GFP-tubulin z-maximum projection in an elongated (hydroxyurea treated) *klp5*Δ*klp6*Δ cell. **E)** Time for which growing bundle tips were monitored and **F)** number of catastrophes in *klp5Δklp6Δ* cells. We note that f_{cat} measurements in the cytoplasm of *klp5*Δ*klp6*Δ cells are subject to relatively large measurement errors, because due to the low f_{cat} the number of catastrophes in the cytoplasm is smaller than in wild type cells. Statistics at cell poles are comparable to wild type cells

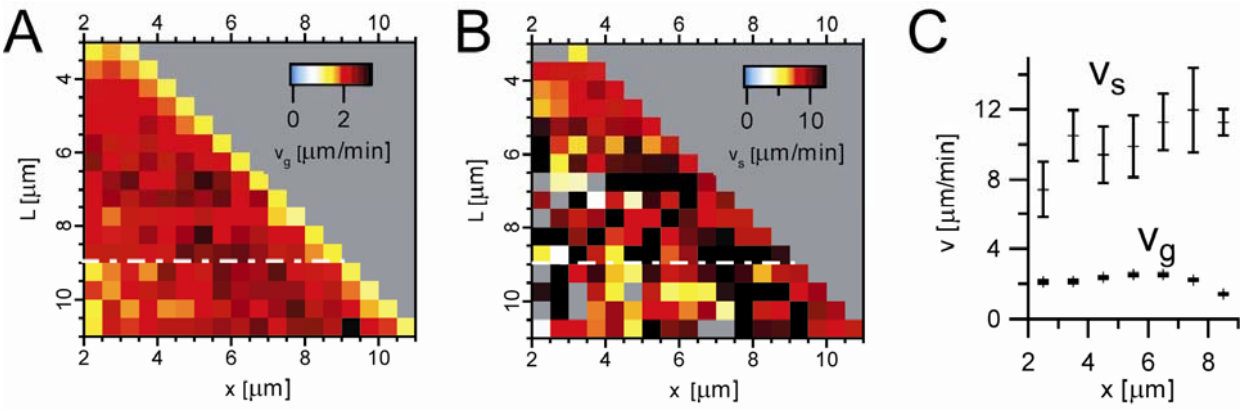

Figure S3 A, B) Bundle tip velocities for growing (v_g) and shrinking (v_s) MTs in *klp5Δklp6Δ* cells. **C)** Velocities for cells with L=9±0.5μm, corresponding to dash-dot horizontal lines in **A** and **B**.

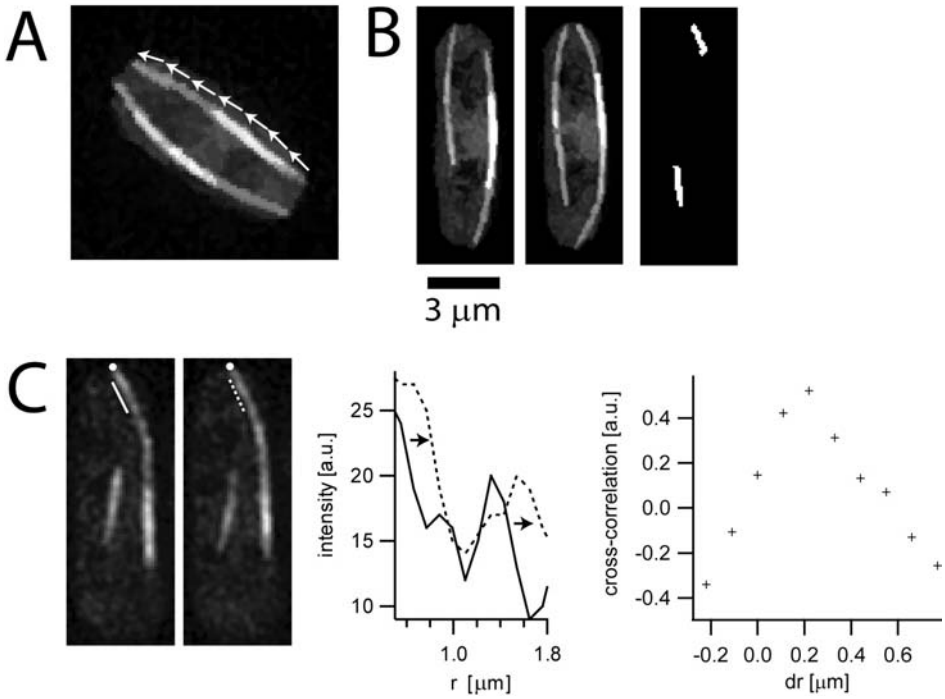

Figure S4 Opposite bundle tip detection and bundle growth measurements. **A)** Image of GFP-tubulin expressing cell with arrows depicting how the algorithm sequentially approaches the opposite bundle tip (see text). **B)** Left: two subsequent images of GFP-tubulin with a time delay of 24s. Right: white areas correspond to automatically detected bundle growth as occurring during the two subsequent images. **C)** Left: two subsequent images of GFP-tubulin with a time delay of 8s. Middle: intensity profiles along the bundle tips indicated by the white lines in the two subsequent images. Right: cross-correlation of the two intensity profiles. (Note: the first two panels in C are identical to Figure 4D in the main text.)

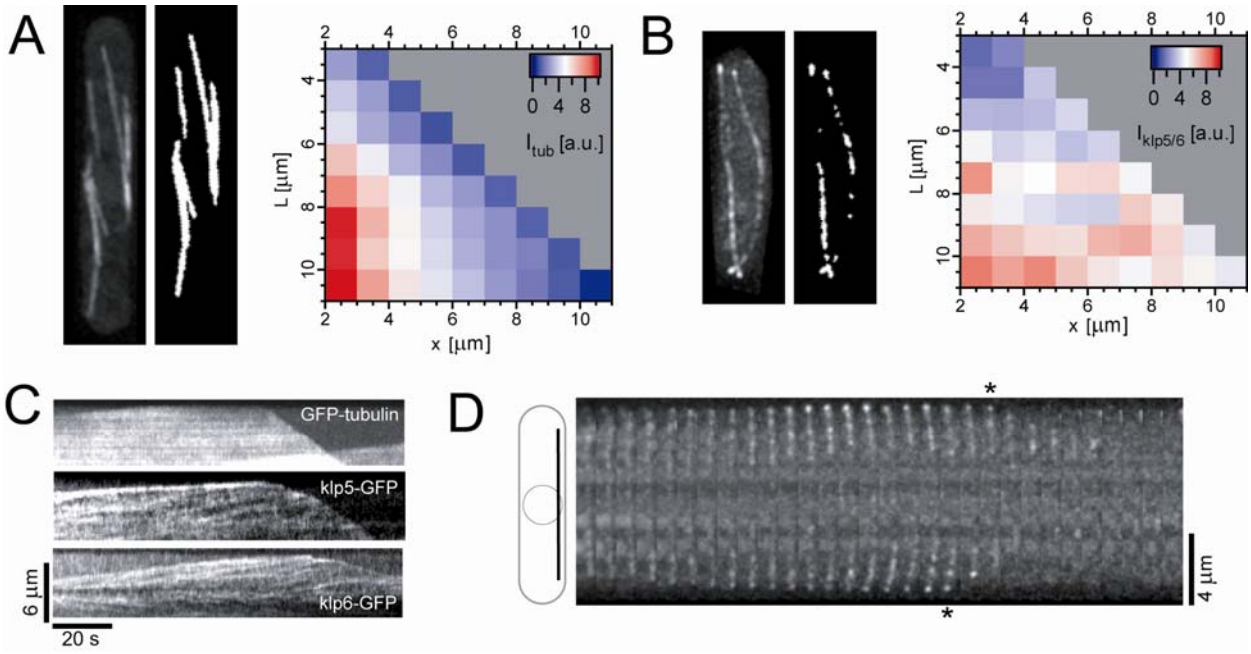

Figure S5 Klp5-GFP and Klp6-GFP localization and dynamics in interphase fission yeast cells. **A)** Left: GFP-tubulin z-maximum projection. Middle: mask of all pixels that are brighter than twice the cellular background intensity. Right: average sum of GFP-tubulin pixels that are twice as bright as the cellular background as a function of intracellular position *x* and cell half length *L*; see text for details. **B)** As in A but for Klp5/6-GFP; the example cell shown expresses Klp5-GFP. **C)** Kymographs recorded in a single confocal plane (Δt=500ms) showing speckle motion of the indicated constructs in elongated hydroxyurea treated cells; the cell pole is at the top of each kymograph (overall intensities decrease in the course of time due to photo-bleaching). **D)** Time series of z-maximum projections, showing Klp5-GFP accumulating at the tips of a MT bundle. The stars indicate moments of catastrophes. Time between images is 4 seconds.

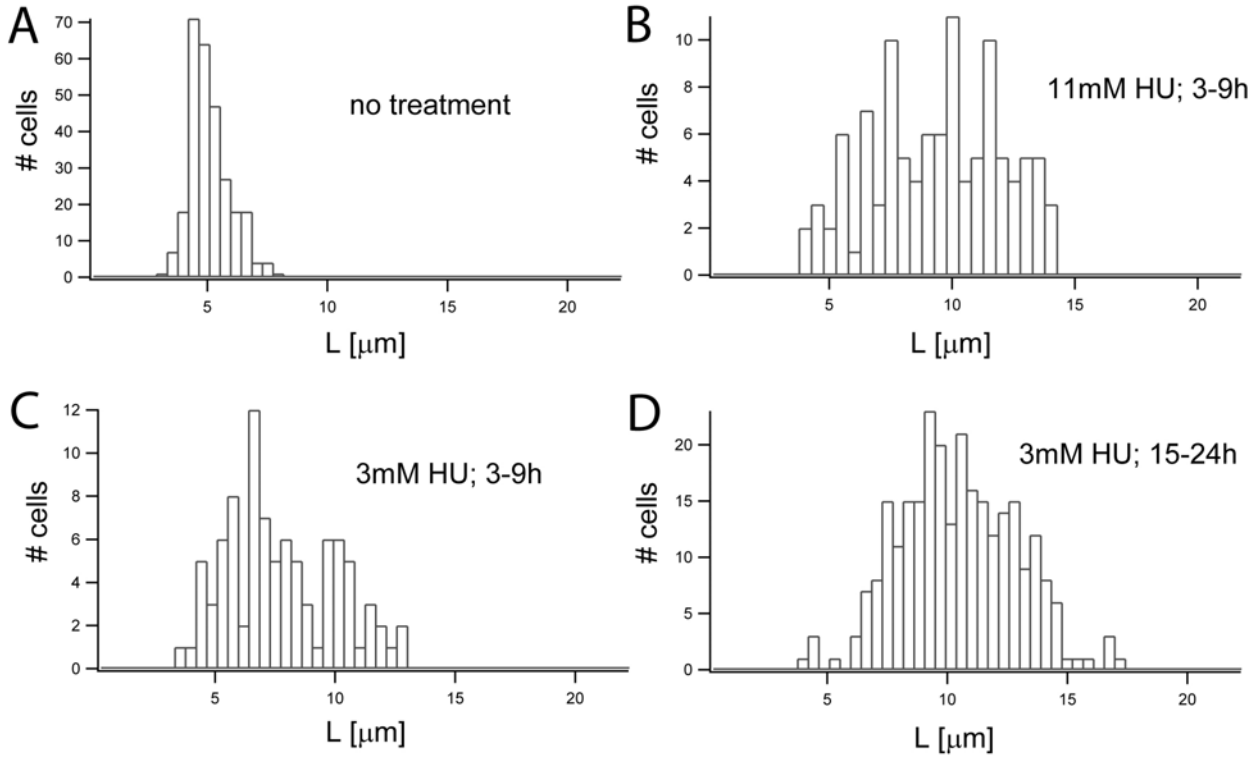

Figure S6 Hydroxyurea treatment **A-D)** Cell length distributions for cells treated with the indicated hydroxyurea concentration for the indicated time.

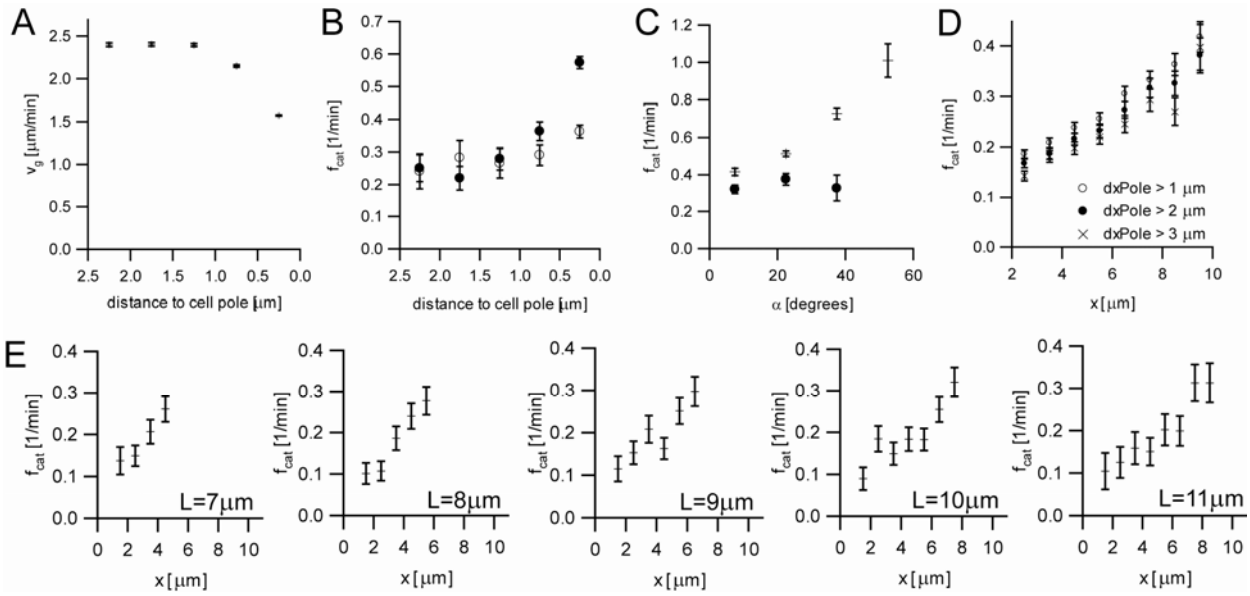

Figure S7 Additional analyses on spatial dependence of MT catastrophes. **A)** Additional information regarding data as shown in Figure 3A&C in the main text. Bundle tip velocities for growing (v_g) microtubules as a function of distance to the cell pole (averaged for all cell lengths L<7µm). **B)** More detailed analysis of results as shown in Figure 3B&C in the main text. Catastrophe frequency depending on bundle tip distance to the cell pole and depending on position of the opposite bundle tip. Closed circles: opposite bundle tip is within opposite cell pole region. Open circles: opposite bundle tip is not within opposite cell pole region. **C)** Additional analysis regarding data as shown in Figure 3F&G in the main text. F_{cat} as a function of the angle between bundle tip and the long axis of the cell. Crosses: MTs that are within the cell pole region; same data as in the main text. Circles: MTs that are between 0.5 and 1 µm from the cell pole region; as angles larger than 45 degrees rarely occur, there is no f_{cat} measurement for large angles. **D)** Additional analysis regarding the lower trace in Figure 2B in the main text. F_{cat} at the pole of cells of different lengths ($x=L$). Different traces show f_{cat} in the cytoplasmic region at position x, averaged over all cells with $L>x+dxPole$. This means that only events that are more than *dxPole* away from the cell pole are taken into account. *dxPol*e = 1µm corresponds to the data shown in the main text. **E)** F_{cat} as a function of distance to the cell center for cells of the indicated half-lengths $L\pm\Delta L$ with $\Delta L=0.5$µm. Only events that were more than 2 µm away from cell poles were included in this analysis.

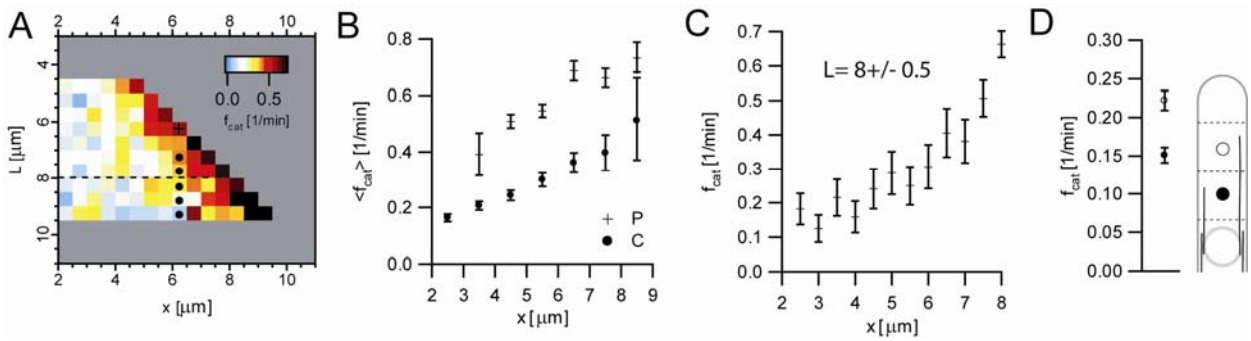

Figure S8 Spatially resolved f_{cat} measurements in a CDC25-22 mutant strain where, also at room temperature, cells are on average longer than in wild type cells (strain: h-cdc25-22 lys1+::nmt1-GFP-atb2, imaged at 25° Celsius). **A)** $f_{cat}(x,L)$; The cross and the circles refer for one specific x to the presentation of the data in B. Dashed horizontal line indicates data shown in C. Statistics: N_{cat}=3323; N_{cells}=258. **B)** Crosses: f_{cat} at the poles of cells of different lengths (x=L). Circles: f_{cat} in the cytoplasm at position x, averaged over all cells with L>x+1µm. **C)** $f_{cat}(x)$ for cells with L=8±0.5µm. **D)** Average f_{cat} in cytoplasmic regions proximal (p_{min}<x<p_{max}) and distal (d_{min}<x<d_{max}) to the cell center. p_{min}=1.5µm; d_{max}=L-2µm; p_{max}=d_{min}=(p_{min}+d_{max})/2.

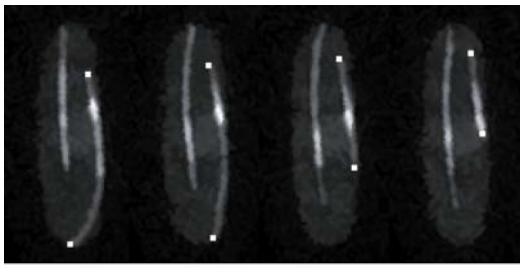

Figure S9 Example time series of GFP-tubulin z-maximum projections, showing a MT bundle that is bent and undergoes a catastrophe while only one bundle tip is contacting a cell pole. Dots indicate the tips of the bundle. Time between images is 16 seconds.